

❸Simulation, Modeling, and Dynamically Based Parameterization of Organized Tropical Convection for Global Climate Models

MITCHELL W. MONCRIEFF, CHANGHAI LIU, AND PETER BOGENSCHUTZ

National Center for Atmospheric Research,^a Boulder, Colorado

(Manuscript received 3 June 2016, in final form 19 January 2017)

ABSTRACT

A new approach for treating organized convection in global climate models (GCMs) referred to as multiscale coherent structure parameterization (MCSP) introduces physical and dynamical effects of organized convection that are missing from contemporary parameterizations. The effects of vertical shear are approximated by a nonlinear slantwise overturning model based on Lagrangian conservation principles. Simulation of the April 2009 Madden-Julian oscillation event during the Year of Tropical Convection (YOTC) over the Indian Ocean using the Weather Research and Forecasting (WRF) Model at 1.3-km grid spacing identifies self-similar properties for squall lines, MCSs, and superclusters embedded in equatorial waves. The slantwise overturning model approximates this observed self-similarity. The large-scale effects of MCSP are examined in two categories of GCM. First, large-scale convective systems simulated in an aquaplanet model are approximated by slantwise overturning with attention to convective momentum transport. Second, MCSP is utilized in the Community Atmosphere Model, version 5.5 (CAM5.5), as tendency equations for second-baroclinic heating and convective momentum transport. The difference between MCSP and CAM5.5 is a direct measure of the global effects of organized convection. Consistent with TRMM measurements, the MCSP generates large-scale precipitation patterns in the tropical warm pool and the adjoining locale; improves precipitation in the intertropical convergence zone (ITCZ), South Pacific convergence zone (SPCZ), and Maritime Continent regions; and affects tropical wave modes. In conclusion, the treatment of organized convection by MCSP is salient for the next generation of GCMs.

1. Introduction

Organized deep convection involving two-way interaction between multiscale cloud systems and their environment affects weather and climate in ways that are inadequately treated by global climate models (GCMs). It is essential to alleviate such deficiencies in order to address challenging physical and dynamical issues such as the intersection between weather and climate at subseasonal time scales, the effects of climate variability on weather extremes, and the role of the atmospheric water and energy cycle manifested by the distribution, type, and intensity of precipitation on regional and global scales (Moncrieff and Waliser 2015).

Excellent progress has been made with our observational, numerical, and theoretical understanding of organized convection, notably mesoscale convective systems (MCSs), but the treatment of organized convection in GCMs has languished with few exceptions (e.g., Donner 1993; Donner et al. 2001; Mapes and Neale 2011). A likely contributing factor is the perceived complexity of organized convection that has daunted attention or stifled interest in this fundamental and practical issue. We obviate this perception by taking a dynamical systems approach called multiscale coherent structure parameterization (MCSP) inaugurated in a minimalist way in a state-of-the-art GCM.

The resolution of contemporary GCMs is too coarse to treat MCSs explicitly and convection parameterizations fail to account for the distinguished properties of environmental shear. For example, the latent heat released in the upper-tropospheric stratiform region of MCSs and the heat absorbed by the evaporation of precipitation in mesoscale descent cause “top heavy” convective heating that affects the large-scale tropical circulation (e.g., Hartmann et al. 1984; Schumacher et al. 2004). In dynamical respects, the countergradient vertical transport of horizontal momentum by organized

❸ Denotes content that is immediately available upon publication as open access.

^aThe National Center for Atmospheric Research is sponsored by the National Science Foundation.

Corresponding author e-mail: Dr. Mitchell W. Moncrieff, moncrief@ucar.edu

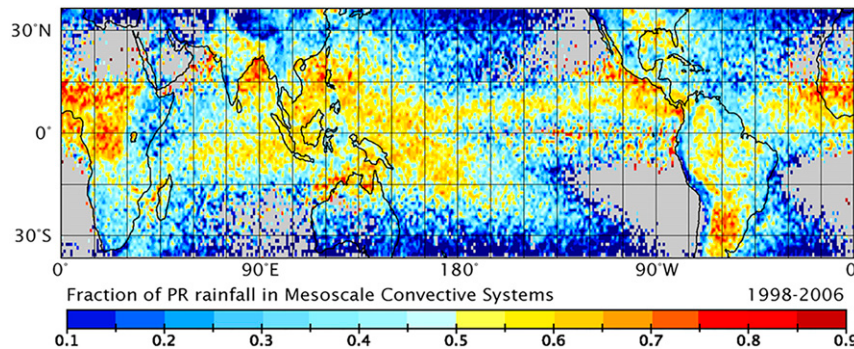


FIG. 1. Fraction of MCS precipitation derived from TRMM precipitation radar measurements for the tropics and subtropics. The darker orange and red hues denote precipitation features on horizontal scales of order 100 km, the stratiform regions of MCS embedded in large-scale meteorological features in the western Pacific warm pool, the ITCZ, SPCZ, and downstream of significant orography. From Tao and Moncrieff (2009), adapted from Nesbitt et al. (2006).

convection in sheared environments and the associated upscale transport of kinetic energy (Moncrieff 1981) is a form of “backscatter” shown to affect predictability (Berner et al. 2009). We refer to Houze (2004, 2014), Moncrieff (2010), and Moncrieff et al. (2012) for comprehensive descriptions of convective organization and its representation in global weather and climate models.

Analysis of Tropical Rainfall Measuring Mission (TRMM) precipitation radar data (Fig. 1) shows MCSs are extensively embedded in large-scale meteorological phenomena that severely challenge GCMs: for example, the Asian–Australian monsoon, Madden–Julian oscillation (MJO), intertropical convergence zone (ITCZ), and South Pacific convergence zone (SPCZ). The Nakazawa (1988) analysis of geostationary satellite data identified hierarchical features of the MJO that GCMs strive to represent, notably the eastward-moving envelope with embedded superclusters and convective systems on 60-, 14-, and 2-day time scales, respectively. The 60-day variability lies beyond the limit of atmospheric predictability. However, the MJO can now be maintained in the ECMWF extended-range prediction system for about a month, a remarkable advance compared to 20 days just a few years ago (Vitart 2014). Meeting the challenge of prediction beyond the 14-day range at the intersection of weather and climate is a key objective of the World Weather Research Programme (WWRP)–World Climate Research Programme (WCRP) Subseasonal-to-Seasonal (S2S) prediction project (Vitart et al. 2015) where organized convection has a prominent place.

The interaction between organized convection and convectively coupled equatorial waves (CCEWs) affects tropical variability in various ways (Kiladis et al. 2009). The similar morphology of organized convection across scales, called scale invariance or self-similarity, is widely observed in the tropics. Based on linear wave theory,

Takayabu (1994) explained the self-similarity of CCEWs in terms of a common equivalent depth (about 20 m). Takayabu et al. (1996) addressed the self-similarity of tropical cloud ensembles in a quasi-2-day wave context. Mapes et al. (2006) advocated mesoscale convection as building blocks for larger-scale tropical systems. Johnson et al. (1999) categorized convection in the tropical western Pacific into cumulus congestus, deep convection, and stratiform cloud types. This categorization is utilized in the development of a multicloud model (MCM) parameterization by Majda (2007), Khouider and Majda (2006, 2007, 2008), and Biello et al. (2010). We provide a physical and dynamical basis for self-similarity that has important implications for the parameterization of organized convection in GCMs.

Global weather prediction models have more success with organized convection than GCMs owing to their higher resolution and the assimilation of a vast amount of data, especially satellite measurements. The ECMWF Integrated Forecast System (IFS), recently upgraded to a 9-km computational grid, treats MCS propagation over the continental United States with considerable fidelity (Moncrieff and Waliser 2015, their Fig. 7). As far as resolution is concerned, a 10-km grid is arguably an upper bound or threshold for the explicit treatment of MCSs. Moncrieff and Liu (2006) showed that a 3-km-grid cloud-system-resolving model (CRM) simulates MCSs and a 10-km grid permits MCSs with reduced amplitude. On the other hand, a 30-km grid causes serious structural distortion such as upright mesoscale ascent and the absence of mesoscale descent.

CRMs with global computational domain simulate convective organization on meso- to global scales. The Nonhydrostatic Icosahedral Atmospheric Model simulates convective momentum transport (Miyakawa et al. 2012), which is difficult to obtain from field-campaign

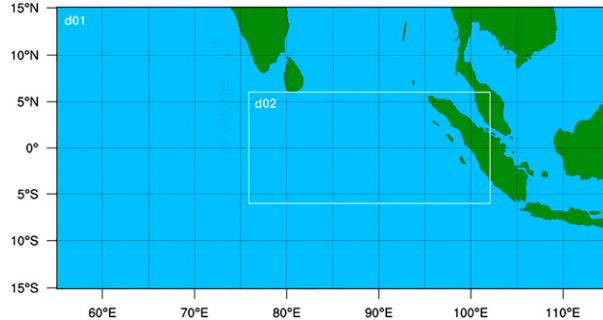


FIG. 2. Plan view of the WRF Model nested domains d01 and d02, at 4- and 1.3-km grid spacing, respectively.

data (e.g., Tung and Yanai 2002). Organized convection is explicit but far from perfect in superparameterized models (Grabowski 2001; Khairoutdinov et al. 2005). The periodic lateral boundary conditions imposed on CRMs that replace traditional convection parameterizations in these models confine MCSs to their domains of birth. Interaction between convective heating in the CRM domains and environmental shear generates large-scale cloud systems on the climate grid as described in sections 4a and 5a herein.

We propose MCSP as an organized convection parameterization for GCMs that utilizes nonlinear dynamical models as transport modules. This paradigm has affinity with the Khouider–Majda MCM approach. The important distinction is that MCM replaces the entire parameterization whereas MCSP adds heating and momentum transport by organized convection to cumulus parameterization. Therefore the large-scale effects of organized convection are simply the difference between GCM simulations with and without MCSP.

The presentation of this paper is as follows. Section 2 defines the CRM configuration, and section 3 describes the simulated convective systems embedded in equatorial waves and the MJO. Section 4 summarizes Lagrangian-based slantwise overturning models of organized convection as a rigorous dynamical basis for the observed self-similarity of tropical precipitation systems across scales. Section 5 evaluates slantwise overturning in a superparameterized aquaplanet model and defines the minimalist treatment of the MCSP incorporated in the NCAR Community Atmosphere Model (CAM). The paper concludes in section 6 with a description of the next steps in the dynamical systems approach to the parameterization of multiscale convective organization in GCMs.

2. Configuration of the numerical model

Simulation of multiscale convective organization and interactions for the April 2009 MJO utilizes the Weather

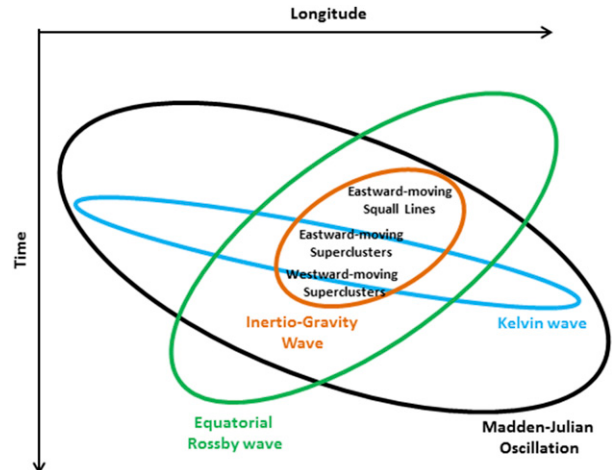


FIG. 3. Idealization of Fig. 4 from Waliser et al. (2012) showing a Hovmöller diagram of the wave modes involving a westward-moving supercluster are embedded in the westward inertio-gravity wave (orange) and an eastward-moving MCS family (red).

Research and Forecasting (WRF) Model, version 3.5.1. Two nested WRF domains (Fig. 2), d01 and d02, span the 15°S–15°N, 55°–115°E and 6°S–6°N, 75°–102°E regions at 4- and 1.3-km grid spacing, respectively. Encouraged by the usefulness of short simulations for parameterization development (Xie et al. 2012), we simulate multiscale convective organization for two short periods, 5–11 and 9–11 April, in the d01 and d02 domains, respectively.

The subgrid parameterizations in WRF are Thompson et al. (2008) for cloud microphysics, Yonsei University (YSU) for the planetary boundary layer (Hong et al. 2006), the Rapid Radiative Transfer Model (RRTM; Iacono et al. 2008), and the Noah land surface model (Chen and Dudhia 2001). ECMWF global analysis provides the initial and lateral boundary conditions. Spectral nudging was applied to the geopotential, wind, and temperature fields in the d01 domain above the planetary boundary layer. A wavenumber threshold of 3 and 2, corresponding to a cutoff wavelength of about 2200 and 1700 km, was selected for the zonal and meridional directions, respectively.

3. Simulated convective organization and tropical-wave interaction

The Year of Tropical Convection (YOTC) virtual global field campaign (May 2008–April 2010) is a unique documentation of organized tropical convection in El Niño and La Niña conditions at 25-km grid spacing (Moncrieff et al. 2012; Waliser et al. 2012; Moncrieff and Waliser 2015). Six MJO events are “observed” in the form of 6-hourly global analyses from the ECMWF IFS. A complex juxtaposition of organized convection and

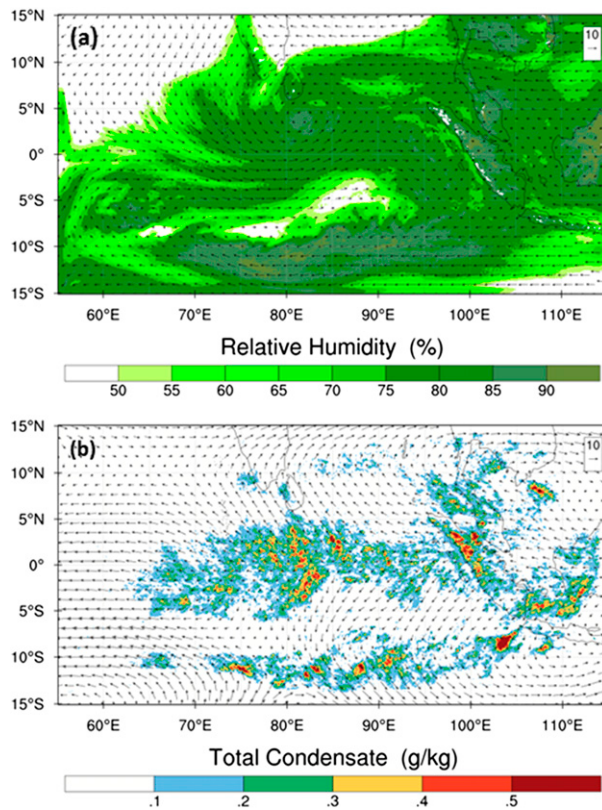


FIG. 4. Fields averaged over 7–10 Apr 2009 for outer domain (d01) of WRF simulation. (a) Relative humidity and wind vectors at 850 hPa. (b) Condensate and wind vectors at 250 hPa.

tropical waves occurred during the 8–11 April period (Fig. 3). A Kelvin wave originated over the Atlantic and a westward-moving equatorial Rossby (ER) emerged from deep convection over the central Pacific. The MJO initiated over the western Indian Ocean, disintegrated over the Maritime Continent, and briefly reorganized in the western Pacific prior to a rapid demise in the prevailing La Niña conditions. A westward-moving inertio-gravity (WIG) wave interacted strongly with an embedded supercluster. The propagation speeds of the ER wave and the WIG wave are about 8.5 and 10 m s^{-1} , respectively. An eastward-moving supercluster is embedded in the Kelvin wave, and the westward-moving supercluster in a westward-moving inertio-gravity wave. While the simulated regimes of convective organization differ in detail, all exhibit the rearward-slanted morphology and top-heavy heating of observed tropical systems (e.g., Takayabu 1994; Takayabu et al. 1996; Haertel and Johnson 1998; Haertel and Kiladis 2004; Lin et al. (2004; Haertel et al. 2008).

The multiscale convective organization and tropical wave interaction associated with the April 2009 MJO

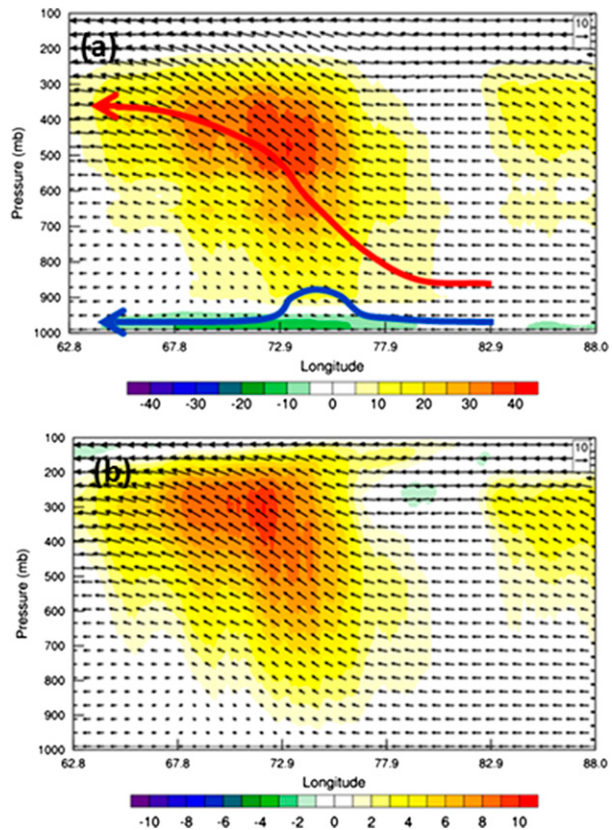


FIG. 5. Fields averaged in an eastward-moving framework between 0600 UTC 6 Apr and 0600 UTC 8 Apr 2009 for 1°S – 1°N in the outer domain (d01) of the WRF simulation. (a) Latent heating (K day^{-1}); (b) vertical velocity (cm s^{-1}). The system is quasi-horizontal because the vertical velocity is magnified by a factor of 20 to assist visualization.

simulated by WRF are classified into the three categories discussed below.

a. Eastward-propagating supercluster embedded in the Kelvin wave

Figure 4a shows the moist lower troposphere, lower-tropospheric convergence, and westerly wind bursts of the MJO and ER wave environment. However, the cyclonic circulation is stronger in the Northern Hemisphere than in the Southern Hemisphere, and the cross-equatorial flow is suggestive of a mixed Rossby–gravity wave rather than asymmetric Rossby wave. In Fig. 4b a bow-shaped supercluster is centered at about 80°E . The similar propagation speeds of the supercluster and the Kelvin wave (about 10 m s^{-1}) implies strong interaction between these phenomena. The westward relative inflow at all levels means that the supercluster propagates eastward in a wavelike manner. The morphology of the top-heavy latent heating above a shallow evaporation-cooled layer (Fig. 5a) closely resembles that of the

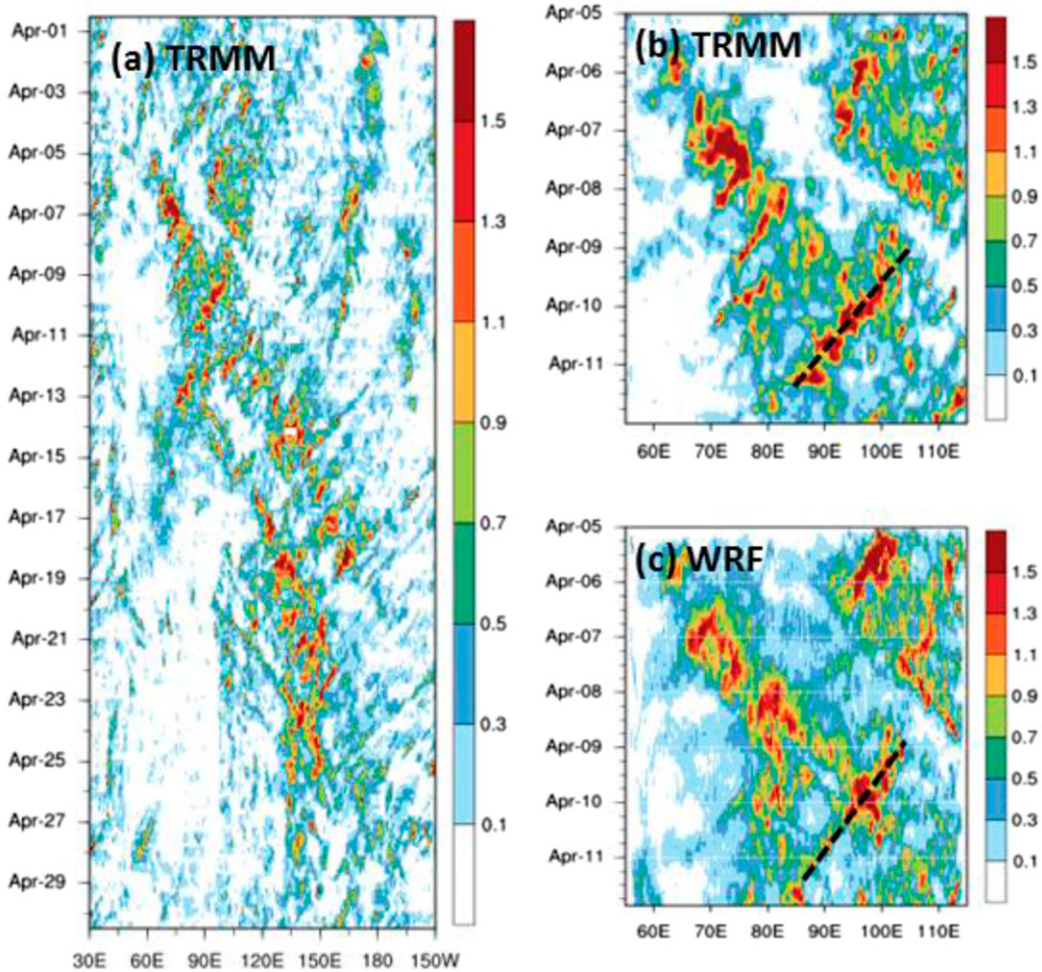


FIG. 6. The 10°S – 10°N -averaged rain rate (mm h^{-1}). (a) TRMM observations for 1–30 Apr 2009. (b) TRMM observations for 5–12 Apr 2009. (c) WRF simulation in outer domain (d01).

vertical velocity (Fig. 5b). Averaged over a wider meridional region, the morphology is similar but with decreased intensity (not shown).

b. Westward-moving supercluster embedded in the westward-moving inertio-gravity wave

The Hovmöller diagram in Fig. 6a shows an eastward-moving envelope and westward-moving systems in the eastern Indian Ocean during 9–11 April. The retrogressive propagation of the convective envelope and the embedded systems is a structural feature of different wave categories—for example, the Kelvin wave case analyzed by Straub and Kiladis (2002) and the hierarchical structure of MJOs (Nakazawa 1988). However this dynamical behavior is not represented by convective parameterization, unless organized features such as mesoscale downdrafts are included (e.g., Yano et al. 1995, their Fig. 3). The TRMM 3B42 measurements and

the WRF simulations in Figs. 6 and 7 show excellent agreement. The westward-moving disturbance and the supercluster have similar horizontal scales (about 1300 km) as shown by 0600 UTC 10 April–0600 UTC 11 April average (Fig. 8). The high resolution in the d02 domain (1.3-km grid) compared to the TRMM 3B42 database (about 25 km) is the reason for the greater detail in Fig. 7.

The cross-equatorial flow and the convergence–divergence dipole at the lower and upper levels (not shown) associated with the WIG wave qualitatively resembles the Matsuno (1966) idealized model. The wave travels at about 10 or 20 m s^{-1} relative to the lower-tropospheric zonal wind. The rearward slant of the supercluster with warm ascent overlying cool descent (Figs. 8a,b) reveals a second-baroclinic vertical structure resembling quasi-2-day waves (Takayabu 1994; Takayabu et al. 1996; Kiladis et al. 2009). Figure 8c shows the

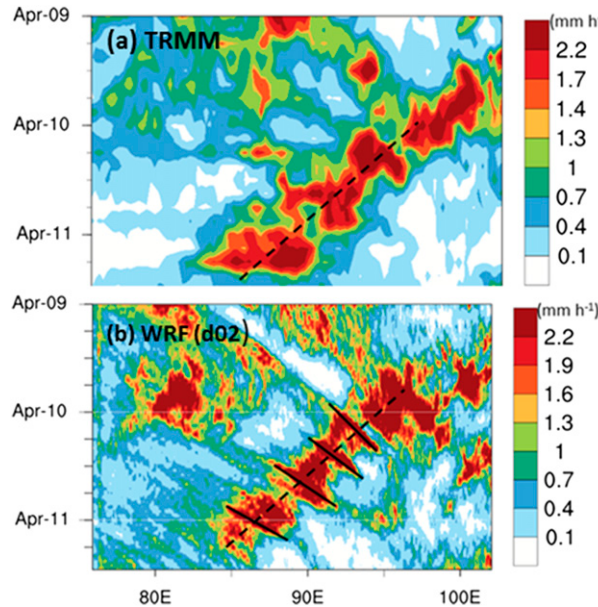


FIG. 7. The 5°S – 5°N -averaged rainfall rate. (a) TRMM. (b) WRF inner domain (d02).

meridional- and time-averaged vertical cross section of the convective heating (condensation and sublimation) overlying a shallow cold pool. The latent heating associated with the inertio-gravity wave and the supercluster is markedly top heavy. The self-similarity of the supercluster and the WIG structure implies strong convection–wave interaction or, arguably, a collective manifestation.

c. Eastward-propagating tropical squall lines

Figures 9a–d shows four tropical squall lines within the WIG wave traveling eastward/southeastward at speeds ranging from 8.5 to 12 m s^{-1} . Although the TRMM 3B42 measurements cannot resolve the squall lines, their presence in the form of higher rain rates is indicated by the continuous black lines in Fig. 7b. The squall lines and the inertio-gravity wave do not strongly interact perhaps because they travel in opposite directions and therefore fail to reinforce each other. The vertical cross sections in Figs. 9e–g with one-sided system-relative mesoscale inflow at all levels indicate wavelike propagation akin to the synoptic-scale systems in Fig. 5. This provides further evidence for self-similarity.

We now describe a minimalist parameterization of organized convection for GCMs utilizing the Moncrieff (1992, hereafter M92) archetypal models as transport modules for the MCSP. These models have been verified by CRM simulations and field measurements of organized convection in sheared environments (e.g., Houze 2004, 2014; Moncrieff 2010).

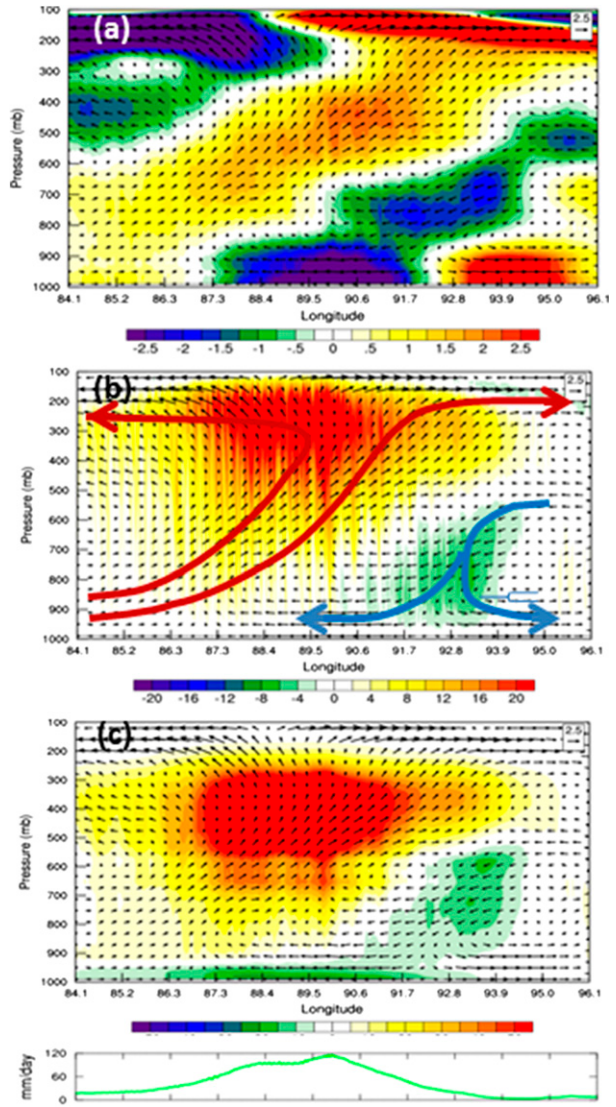


FIG. 8. Cross sections meridionally averaged between 0.5°S and 1.5°N and temporally averaged in system-relative coordinates during 0600 UTC 10 Apr–0600 UTC 11 Apr 2009. (a) Zonal wind perturbation (m s^{-1}) relative to the 0600 UTC 10 Apr–0600 UTC 11 Apr 2009 time mean, (b) vertical velocity (cm s^{-1}), and (c) latent heating (K h^{-1}). (bottom) Precipitation rate (mm day^{-1}).

4. Multiscale coherent structure parameterization

The assumption in traditional cumulus parameterization of a gap or scale separation between the cumulus convection and the GCM grid has long been in conflict with GATE field campaign observations that show the presence of mesoscale systems within the assumed gap (Houze and Betts 1981). Addressing this conundrum was a significant motivation for YOTC's focus on organized tropical convection (Moncrieff et al. 2012).

Figures 10a and 10b show the traditional ensemble-based cumulus parameterization (Arakawa and Schubert

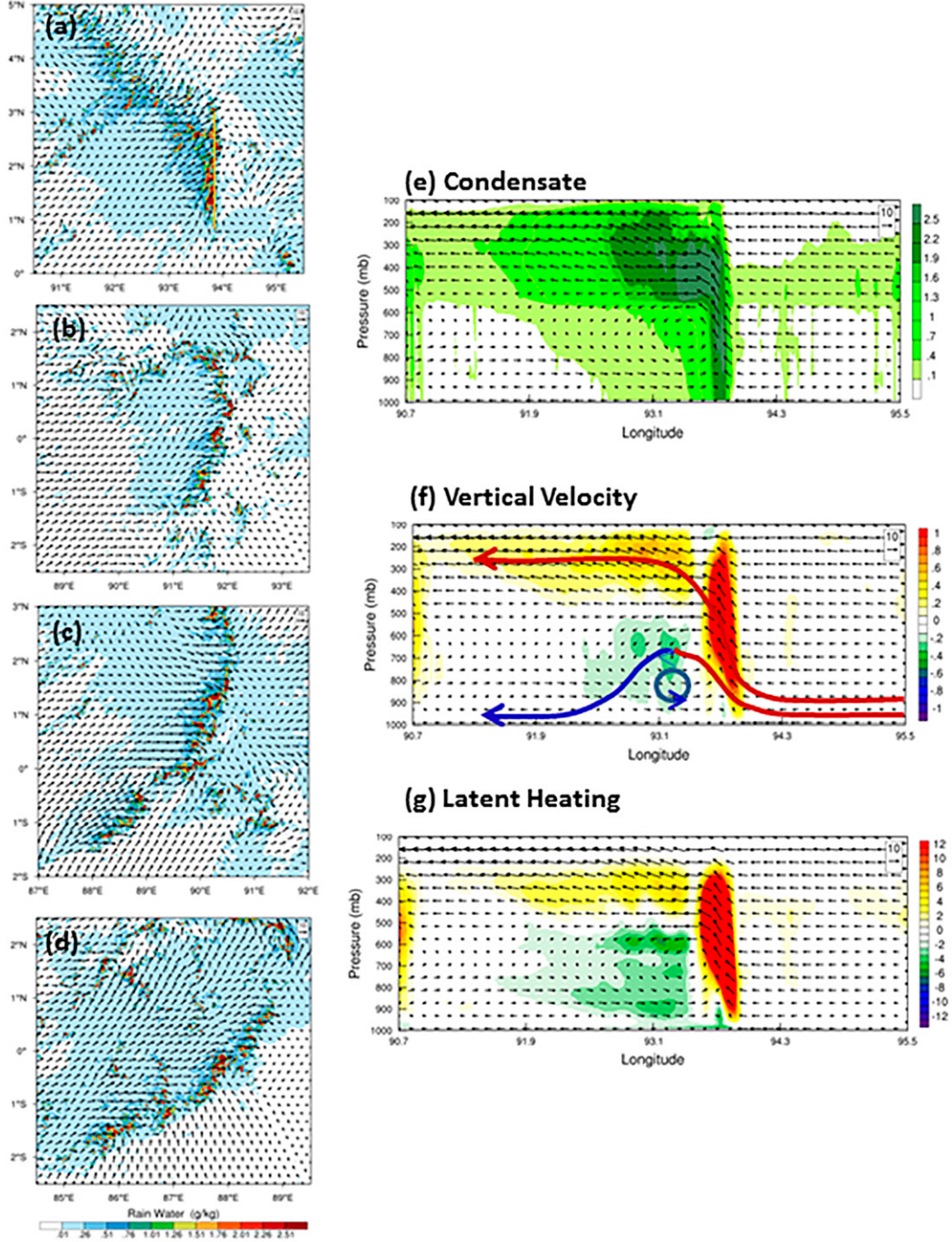


FIG. 9. Snapshots of near-surface condensate (g kg^{-1}) and wind vectors (m s^{-1}) for the four eastward-moving squall lines identified by the black lines in Fig. 7b: (a) 0600 UTC 10 Apr 2009, propagation speed $c = 8.5 \text{ m s}^{-1}$; (b) 11 UTC 10 Apr 2009, $c = 11 \text{ m s}^{-1}$; (c) 17 UTC 10 Apr 2009, $c = 11 \text{ m s}^{-1}$; (d) 0000 UTC 11 Apr 2009, $c = 12 \text{ m s}^{-1}$. (e)–(g) Cross sections for the MCS averaged along the yellow line segment in (a) for condensate (g kg^{-1}), vertical velocity (cm s^{-1}), and latent heating (K h^{-1}), respectively.

1974) but the cumulus elements do not interact and the organizational effects of vertical shear are not taken into account. While environmental shear is accounted for in cumulus momentum transport parameterizations (e.g.,

Wu and Yanai 1994; Kershaw and Gregory 1997; Richter and Rasch 2008) it plays a passive role. Referring to the dynamical systems concept of MCSP (Fig. 10c) organized convection is treated as a multiscale coherent structure

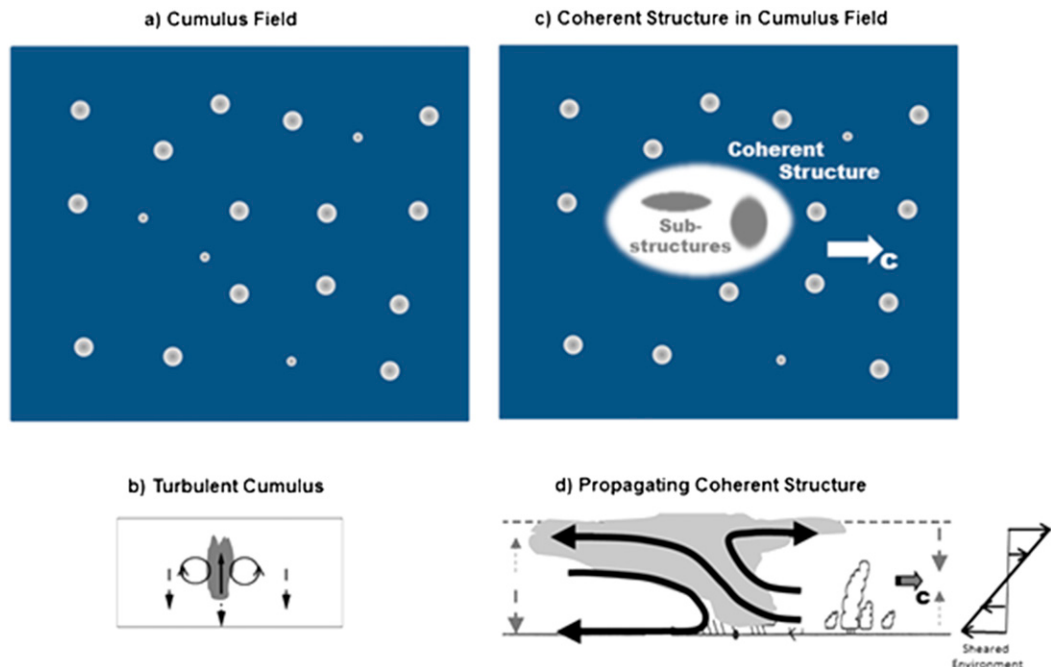


FIG. 10. Distinctions between traditional cumulus parameterization and multiscale coherent structure parameterization. (a) Quasi-random field of cumulus. (b) Single-column entraining plume model with cumulus updrafts and downdrafts and compensating descent. (c) Multiscale coherent structure embedded in a field of cumulus. (d) Propagating slantwise overturning model in a sheared environment with a rearward-tilted circulation and a three-branch circulation: overturning updraft, overturning downdraft, and jumplike flow. Note that the small cumulus slope downshear and organized convection slope upshear. From Moncrieff and Waliser (2015).

in a turbulent environment. The coherence structure is approximated by the slantwise overturning models (Fig. 10d) that exchange atmospheric layers via convectively generated mesoscale circulations absent from traditional parameterizations. Note that in MCSP cumulus is considered part of the turbulent environment.

A challenge facing future generations of GCMs with sub-10-km grid spacing is dealing with convection-permitting resolution in the so-called gray zone. The gray zone is resolution dependent owing to the existence of other organized phenomena on different scales, such as shallow convection and the planetary boundary layer (Gerard 2015). Note that MCSP addresses mesoscale convective organization in sheared environments and provides an unambiguous measure of how mesoscale organization affects the larger scales of motion.

The following two subsections address related aspects of organized convection treated by slantwise overturning. Section 4a presents the formal mathematical basis and section 4b shows that slantwise overturning is self-similar across scales.

a. Slantwise overturning models

Slantwise overturning is based on Lagrangian conservation principles of the steady-state nonlinear equations

of mass, entropy, total energy, vorticity, and momentum [see Eq. (1) of Moncrieff (1981)]. As a transport module, slantwise overturning is distinguished from entraining plumes in cumulus parameterization; for example, (i) scale separation is not assumed; (ii) grid-averaged quantities are nonzero; (iii) the Lagrangian formulation directly links convective transports to mean-state variables, a basic requirement not satisfied by cumulus parameterizations; and (iv) the rearward tilt of slantwise overturning fundamentally affects the vertical profiles of convective heating and momentum transport.

The sole assumption for the slantwise overturning models is that the convective heating rate H is a separable function of the vertical velocity w ; that is, $H = w\Gamma$, where Γ is the moist adiabatic lapse rate (Moncrieff and Green 1972; Moncrieff 1981). The thermodynamic equation can then be expressed as

$$\frac{D\phi'}{Dt} = w(\Gamma - B), \quad (1)$$

where $B = d\varphi_0/dz$ is the static stability and $\varphi'(x, y, z) = \varphi - \varphi_0(z)$ is the perturbation of log potential temperature from the mean state. The separable assumption enables the two-dimensional slantwise

overturning model to be derived as an exact integral of the Boussinesq vorticity equation in system-relative (x, z) coordinates

$$\frac{D\eta}{Dt} + \frac{\partial F}{\partial x} = 0, \quad (2)$$

where $\eta = u_z - w_x$ and $F = g\varphi'$ is the parcel buoyancy. Based on the conservation of mass, the classical streamfunction ψ is defined by $(u, w) = (\psi_z, -\psi_x)$; therefore, $\eta = \nabla^2\psi$. The fundamental theorem of calculus gives

$$wf(\psi, z) = \frac{D}{Dt} \int_{z_0}^z f(\psi, z') dz', \quad (3)$$

where f is a general integrable quantity measured along parcel trajectories ψ and z' is the vertical displacement of ψ from the inflow level $z_0(\psi)$. Using Eq. (3), the expression

$$\frac{\partial F}{\partial x} = \frac{\partial F}{\partial \psi} \frac{\partial \psi}{\partial x} = -w \frac{\partial F}{\partial \psi} = -\frac{D}{Dt} \int_{z_0}^z \left(\frac{\partial F}{\partial \psi} \right)_{z'} dz' \quad (4)$$

allows Eqs. (1) and (2) to be written as complete total derivatives. When integrated along trajectories in a Lagrangian manner, this gives

$$\varphi'(\psi, z) \int_{z_0}^z (\Gamma - B) dz' \quad (5)$$

and

$$\nabla^2\psi = G(\psi) + \int_{z_0}^z \left(\frac{\partial F}{\partial \psi} \right)_{z'} dz'. \quad (6)$$

Equation (6) shows that the vorticity for slantwise overturning is the sum of environmental shear G and vorticity generated by the horizontal gradient of buoyancy. The propagation speed of slantwise overturning is an eigenvalue of Eq. (6), and the corresponding eigenfunction gives the streamfunction field. Referring to Fig. 11a, two dimensionless quantities control organized convection: the convective Richardson number ($R = \text{CAPE}/\text{AKE}$) and the quotient of static and dynamic pressure terms called the Bernoulli number ($E = \text{WPG}/\text{AKE}$). Here, CAPE is the convective available potential energy, $\text{AKE} = (1/2)(U_0 - c)^2$ is the specific kinetic energy of the system-relative surface inflow (with c the propagation speed of the convective system), and $\text{WPG} = \Delta p/\rho$ is the work done by the surface pressure gradient. The above is the mathematical basis for analytic models of mesoscale slantwise overturning shown by the colored trajectories in Fig. 11a. Importantly, the archetypal

models provide a reliable basis for the minimalist category of MCSP.

Defined by $R = 0$, the M92 archetypal models retain the rearward-tilted structure of the more general models. The archetypal models have been validated by observational measurements and CRM simulations (Houze 2004, 2014; Moncrieff 2010; Yano and Moncrieff 2016). Figure 11b illustrates three archetypal slantwise overturning models, two of which approximate the WRF-simulated convective systems. Regime A is characterized by wavelike propagation and represents the eastward-moving supercluster in Fig. 5 and also the two-dimensional analog of the propagating squall lines in Fig. 9. However, the Lane and Moncrieff (2015) model is more appropriate since it is three dimensional. The three-branch regime (regime B) is an analog of the westward-moving supercluster in Fig. 8.

Recall that the separable relationship between vertical velocity and convective heating enables the slantwise overturning models to be integrals of Eq. (6), subject to appropriate boundary conditions. This basic relationship is now shown to be self-similar across scales, meaning that slantwise overturning is multiscale.

b. Dynamical foundation for self-similarity

The self-similarity for organized tropical convection across meso-, synoptic, and large scales is illustrated by three examples. First, considering the strictly propagating regime A in Fig. 11b, the similar morphology of vertical velocity and latent heating implies that constant Γ is an acceptable approximation for the eastward-propagating supercluster (cf. Figs. 5a,b) and an excellent approximation for the simulated tropical squall lines (cf. Figs. 9f,g). Second, constant Γ is appropriate for the westward-moving supercluster (cf. Figs. 8b,c) except near the tropopause where adiabatic cooling due to overshooting cumulonimbus decreases the convective heating. Third, the vertical velocity and convective heating rate (in pressure coordinates) are remarkably similar in the November 2011 DYNAMO sounding analysis and ERA-Interim (Oh et al. 2015; Figs. 2a–d). We now present the results of numerical experiments showing the generation of large-scale convective organization in the tropics, especially the warm pool of the Indian Ocean–tropical western Pacific and neighboring regions.

5. Large-scale effects of MCSP

We examine large-scale coherent convective structures generated by slantwise overturning utilizing two classes of GCM: (i) an aquaplanet model with attention to momentum transport by slantwise overturning demonstrating that the archetypal models are second-baroclinic

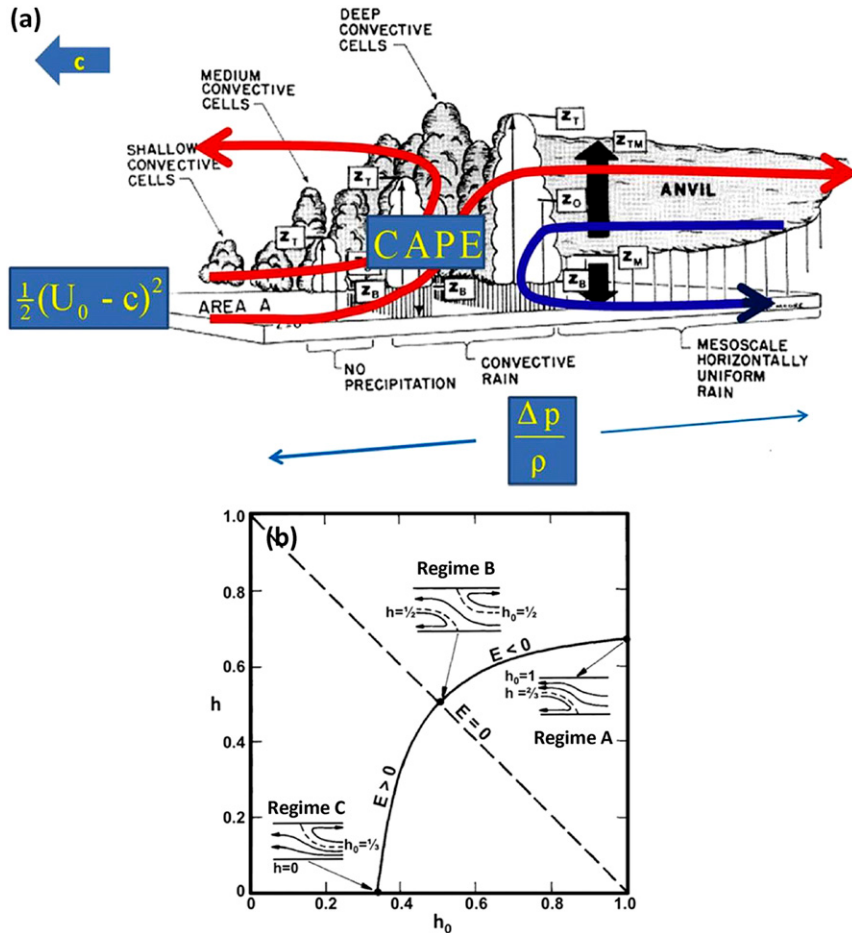


FIG. 11. (a) Standard observational description of an MCS propagating leftward (Houze et al. 1980) with shallow cumulus, medium convective cells, and deep convection ahead of a stratiform anvil region and downdraft. The overlying slantwise overturning consists of a jump upbranch, an overturning upbranch, and an overturning downbranch involving three categories of energy, per unit mass: CAPE, the kinetic energy of relative inflow, and the work done by the horizontal pressure gradient. From Moncrieff (2010), adapted from Tao and Moncrieff (2009). (b) Archetypal models of slantwise overturning, and minimalist solutions of Eq. (6). Insets show strict propagation (regime A), three-branch system with downdraft (regime B), and jumplike ascent with no downdraft (regime C). Here h and h_0 are the depths of the mesoscale downbranch and the jump upbranch, respectively. From Lane and Moncrieff (2015), revised Fig. 2 from M92.

transport analogs for the MCSP and (ii) the effects of second-baroclinic convective heating and momentum transport in the NCAR CAM.

a. Superparameterized aquaplanet model

The Grabowski (2001, hereafter G01) cloud-resolving convection parameterization (CRCP), subsequently dubbed superparameterization, spontaneously generates two categories of large-scale convective organization. Moncrieff (2004, hereafter M04) used his archetypal models to interpret the momentum transport properties associated with convectively coupled supercluster-like

systems and an MJO-like system. The first 40 days of simulation were dominated by wavenumber-4 convectively coupled systems with quasi-symmetric gyres in the horizontal plane and rearward slant in the vertical plane. These systems generate lower-tropospheric easterly and upper-troposphere westerly perturbations with second-baroclinic vertical structure. The archetypal models approximate the vertical transport of zonal momentum.

The MJO-like system that evolves after about 50 days of simulation has a distinct second-baroclinic (two layer) structure. The large-scale coherent structure in the horizontal plane in the upper-level consists of quasi-horizontal

Rossby gyres that resemble actual MJOs. The lower layer has Rossby gyres with meridional-tilted eddies on their poleward flanks. Momentum transport in the meridional plane approximated by the Rossby-gyre archetypal model generates equatorial superrotation. The slantwise overturning in the vertical plane is controlled by the convective Richardson number and the Bernoulli number and slantwise overturning in the horizontal plane by an inverse Rossby number and the Bernoulli number. The respective vorticity equations for the slantwise overturning regimes of organization are identical except the inverse Rossby number replaces the convective Richardson number [cf. M04, their Eqs. (4) and (11)]. In other words, the aquaplanet simulations demonstrate a fundamental self-similarity between convective coherence in the vertical plane and rotational coherence in the horizontal plane. Slantwise overturning circulations are the key link.

The principal conclusions of the aquaplanet analysis are as follows:

- (i) Second-baroclinic heating and mesoscale momentum transport are directly associated with the generation of large-scale coherence.
- (ii) The slantwise overturning models approximate the momentum transport by supercluster-like coherence in the vertical plane and MJO-like coherence in the horizontal plane.
- (iii) A general principle for the multiscale self-similarity of slantwise overturning is based on the equivalence of large-scale coherent structures in the horizontal plane and mesoscale structures in the vertical plane.
- (iv) Second-baroclinic heating and momentum transport are central to the utilization of slantwise overturning as a transport module for MCSP.

There is a dynamical affinity between MCSP and the Khouider–Majda MCM parameterization to be pursued in follow-on research. Khouider and Han (2013) showed the role of momentum transport by mesoscale systems embedded in a Kelvin wave. Biello et al. (2007) showed that equatorial superrotation occurs when the planetary flow due to the upscale vertical momentum transport from synoptic scales reinforces the horizontally convergent flow arising from planetary-scale heating.

The spontaneous generation of large-scale organization by second-baroclinic heating and momentum transport in the aquaplanet model poses a key question: Can MCSP with slantwise overturning as the transport module generate large-scale coherence in a full GCM?

b. Community Atmosphere Model

We utilize the development version of the Community Atmosphere Model, version 5.5 (CAM5.5). The physical parameterizations in CAM5.5 differ in several respects

from CAM5 (Neale et al. 2012). First, the implementation of the Cloud Layers Unified by Binormals (CLUBB; Golaz et al. 2002; Bogenschutz et al. 2013) parameterization replaces the CAM5 planetary boundary layer, shallow convection parameterizations, and also the cloud-macrophysics parameterization. Second, CAM5.5 retains the Zhang and McFarlane (1995) deep convection scheme in CAM5 and incorporates the Richter and Rasch (2008) cumulus momentum transport parameterization. A series of 10-yr CAM5.5 experiments were run with a 0.9° by 1.25° grid in the zonal and meridional directions, respectively. Years 2–10 were analyzed.

As shown by Fig. 11a, slantwise overturning is the mesoscale response of an ensemble of cumulonimbus in sheared environments. Families of cumulonimbus triggered by downdraft outflows mature as they travel $O(100)$ km rearward and sustain a horizontal pressure gradient (Lafore and Moncrieff 1989; Moncrieff and Klinker 1997) that drives a mesoscale circulation identified by the trajectories in Fig. 11a. The work done by the horizontal pressure gradient defines the Bernoulli number that controls the archetypal morphology and transport properties. The dipole-like mesoscale heating in the MCS rear is due to latent heating overlying evaporative-cooled descent (Figs. 12a,b).

The minimalist mesoscale heating has a top-heavy second-baroclinic vertical profile:

$$Q_m(p, t) = -\alpha_1 Q_c(t) \sin 2\pi \left(\frac{p_s - p}{p_s - p_t} \right), \quad (7)$$

where p_s and p_t are the pressure at the surface and top of the stratiform region, respectively. In the following CAM5.5 experiments, the amplitude $\alpha_1 > 0$ of the top-heavy heating Q_m is proportional to the vertical average of the parameterized cumulus heating $Q_c(t)$. The total convective heating is $Q = Q_c + Q_m$. While in reality α_1 is a function of the vertical shear, in our preliminary experiments we assume constant values. Experiments with a first-baroclinic heating added to Eq. (7) generated large-scale precipitation patterns resembling the second-baroclinic results (not shown).

Depending on the horizontal pressure gradient and vertical shear (more precisely, the convective Richardson number and Bernoulli number) the momentum transport by slantwise overturning is upgradient in certain layers and downgradient in other layers (Moncrieff 1997). Upgradient momentum transport increases vertical shear, and the associated upscale transport of kinetic energy transport helps maintain the mean flow against dissipation. For example, an eastward-moving system accelerates the lower-tropospheric flow in the eastward direction and the upper-tropospheric flow in

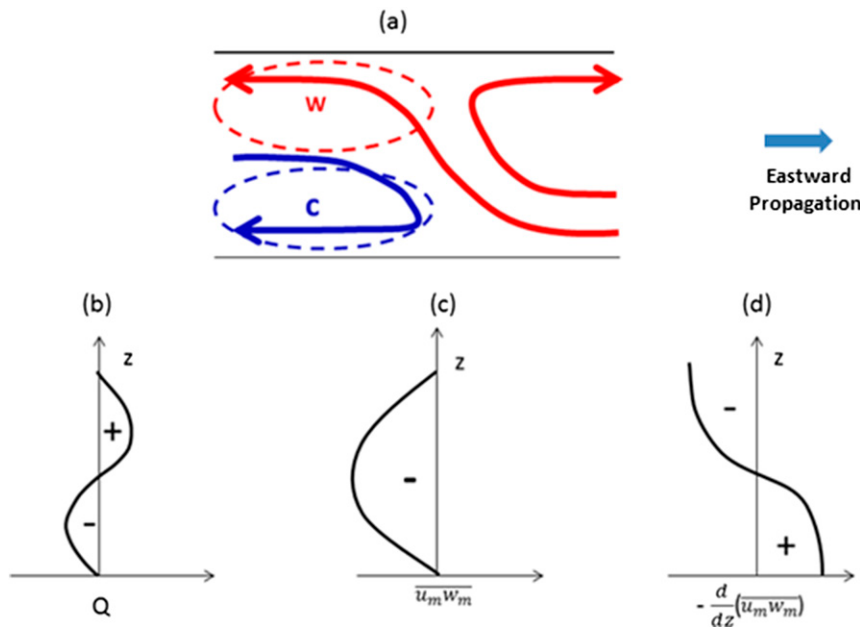


FIG. 12. Rationale for the second-baroclinic mesoscale heating and organized momentum transport tendency in MCSP. (a) Mesoscale heating dominated by warming (W) in the trailing stratiform region and evaporative cooling (C) in the mesoscale descent. (b) Second-baroclinic heating rate. (c) The rearward slant of the trajectories in (a) causes the negative correlation of horizontal velocity u_m and vertical velocity w_m giving a negative momentum transport ($\bar{u}_m \bar{w}_m$) per unit mass. (d) Mesoscale momentum transport tendency is the negative of the vertical gradient of the momentum transport.

the westward direction. Figures 12c,d show the minimalist second-baroclinic momentum transport implemented as the acceleration

$$M_m(p, t) = \alpha_2 \cos\pi \left(\frac{p_s - p}{p_s - p_f} \right), \quad (8)$$

where $\alpha_2 > 0$ and constant values are assumed.

Although the vertical transport of horizontal momentum is three dimensional, the two-dimensional approximation is salient for tropical convection in the warm pool regions where the zonal wind component is dominant and the convectively waves mostly propagate in the zonal direction. Because MCSP adds the “missing process” of slantwise overturning to contemporary cumulus parameterization, the difference (MCSP minus CAM5.5 control) measures the large-scale effects of MCSP. Figure 13 shows that the effects on large-scale precipitation is primarily in the Asian–Australian monsoon, Indian Ocean–western Pacific warm pool, Maritime Continent, SPCZ, and ITCZ regions, consistent with the collocation of MCSs and large-scale systems seen in the TRMM analysis (Fig. 1).

The effects of momentum transport (Fig. 13a) and second-baroclinic heating (Fig. 13b) on the heating rate

are distinctive over the Maritime Continent and the northern part of the SPCZ. Both top-heavy heating and momentum transport decrease the rainfall rate over equatorial Africa. The precipitation rate over the Maritime Continent is reduced by momentum transport but substantially increased by the top-heavy heating (Figs. 13b,c). In most GCMs, and CAM5.5 is no exception, precipitation tends to be excessive in the ITCZ and too spatially continuous. Satellite observations show mesosynoptic variability within the ITCZ, and the decrease in precipitation rate by top-heavy heating is consistent with new instability mechanisms at mesosynoptic scales (Khouider and Moncrieff 2015). Note that the top-heavy heating extends the SPCZ. The average annual precipitation in Fig. 14 is consistent with the above results. That convective heating has more influence than convective momentum transport depends on the prescribed α_1 and α_2 ; clearly, we need observation-based values.

The Fig. 15 Wheeler–Kiladis diagrams (Wheeler and Kiladis 1999) pertain to precipitation rates in the 15°S–15°N equatorial belt. While an 8-yr record is likely too short for meaningful conclusions, the results are encouraging nevertheless. Figure 15a, using NCEP 1971–2000 reanalysis data, shows strong Kelvin waves. While

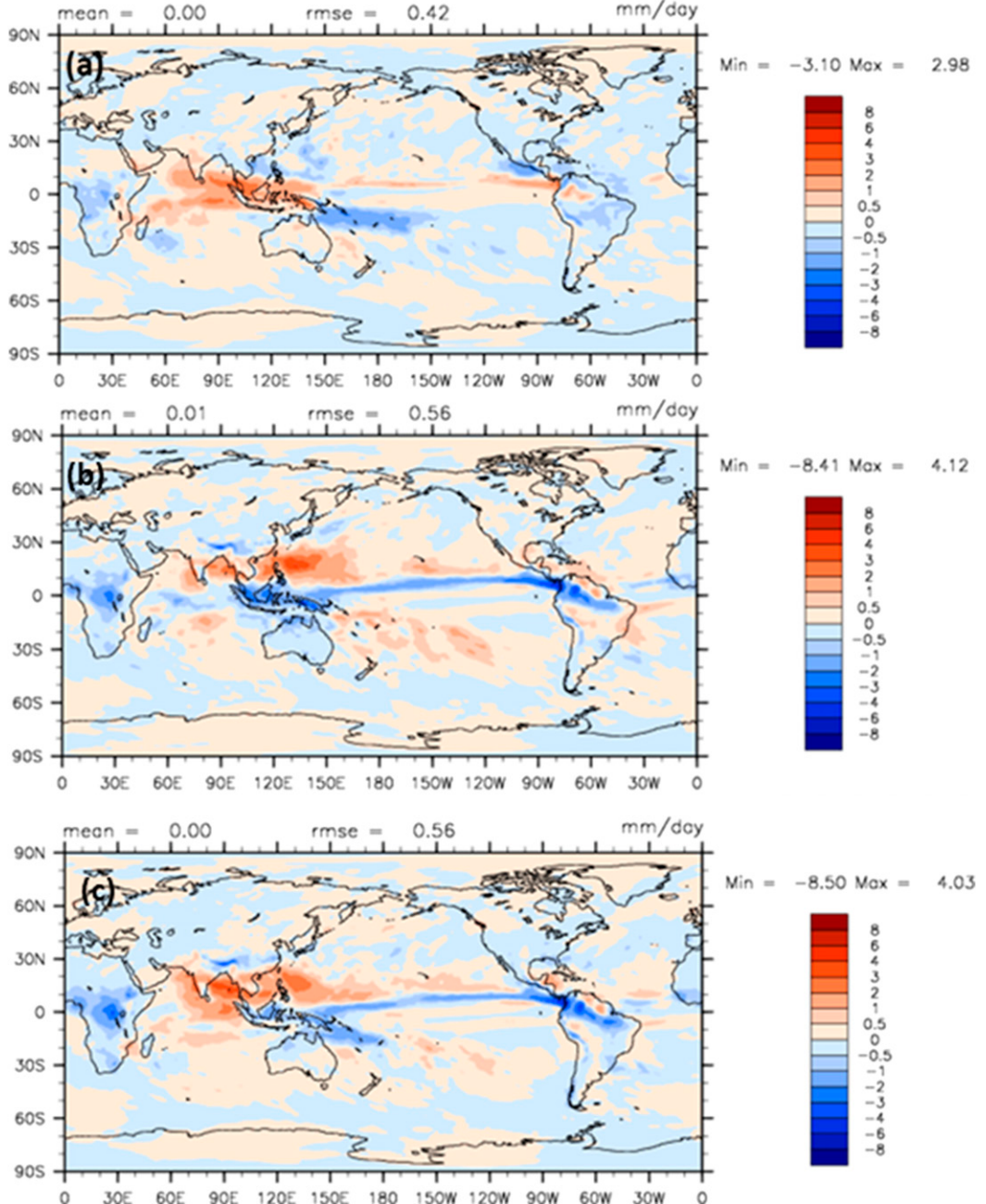


FIG. 13. The 8-yr average of the effects of MCSP on precipitation rate (MCSP minus CAM 5.5 control; mm day^{-1}). (a) Momentum transport experiment, $\alpha_2 = 1 \text{ m s}^{-1} \text{ day}^{-1}$. (b) Second-baroclinic heating experiment, $\alpha_1 = 0.5$. (c) Momentum transport and second-baroclinic heating experiment, $\alpha_2 = 1 \text{ ms}^{-1} \text{ day}^{-1}$ and $\alpha_1 = 0.5$.

CAM5.5 control has a desirably robust MJO signal, the Kelvin waves are weak. The improved MJO in CAM5.5 control compared to earlier versions of CAM may be due to the moister lower troposphere arising from the high entrainment rate in the Zhang and McFarlane parameterization. Note that the MJO is wavenumber 1 in CAM5.5 control, whereas in the NOAA reanalysis it spans

wavenumbers 1–8 with highest amplitude in the wavenumber-1–5 range. Note that wavenumber 1 is consistent with the Majda and Stechmann (2009) “skeleton model” of intraseasonal oscillations deemed a moisture mode. Figure 15c (momentum transport) and Fig. 15d (convective heating) show that MCSP adds wavenumber-2–4 power. It is interesting that effects of momentum

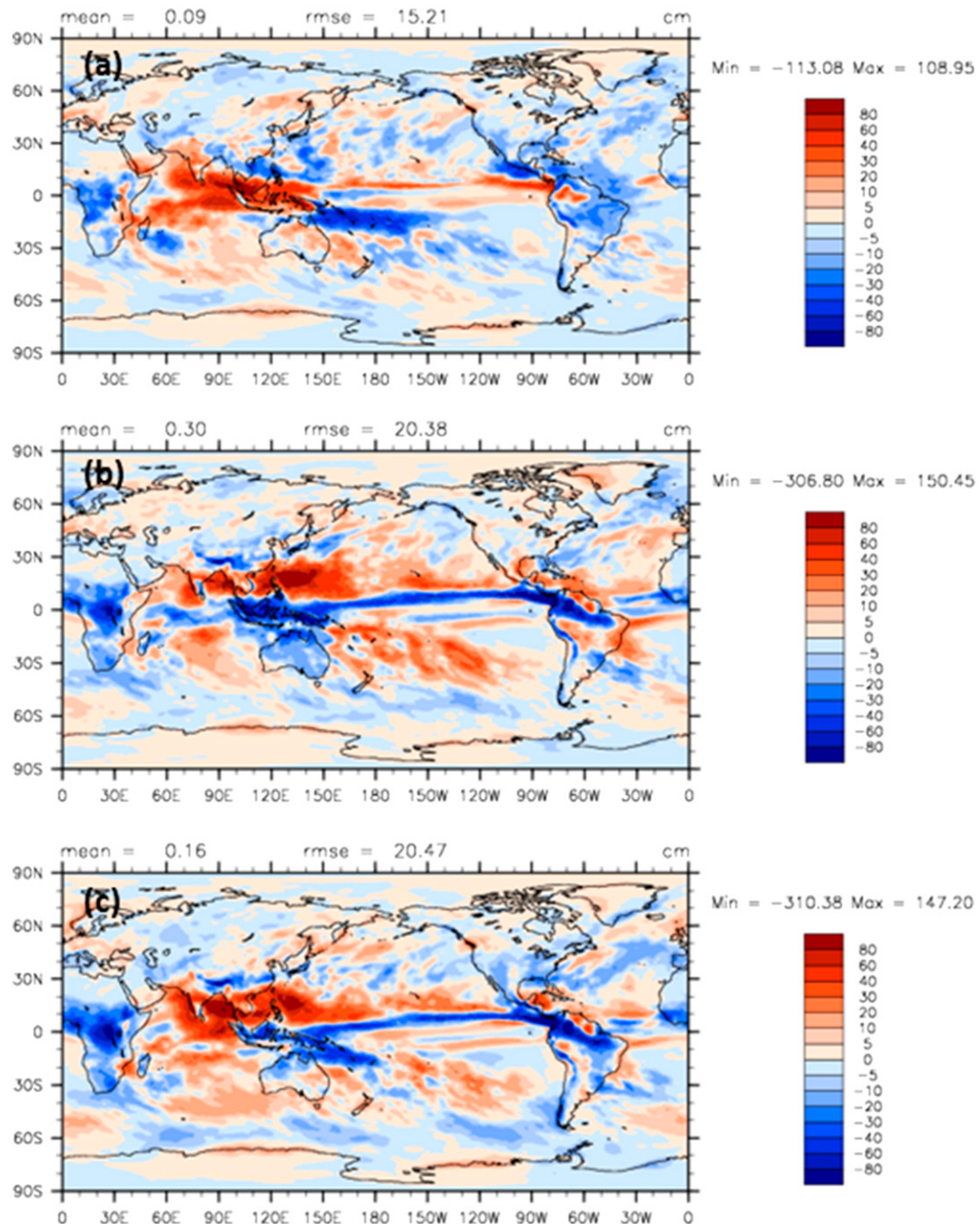


FIG. 14. The 8-yr average of the effects of MCSP on annual precipitation (MCSP minus CAM5.5 control; cm yr^{-1}).
(a) Momentum transport experiment, $\alpha_2 = 1 \text{ m s}^{-1} \text{ day}^{-1}$. (b) Second-baroclinic heating experiment, $\alpha_1 = 0.5$.
(c) Momentum transport and second-baroclinic heating experiment, $\alpha_2 = 1 \text{ m s}^{-1} \text{ day}^{-1}$ and $\alpha_1 = 0.5$.

transport dominate the convective heating in contrast to the Fig. 13 results for precipitation rate.

The positive values of α_2 used here are appropriate for eastward-moving mesosynoptic systems in the MJO and are consistent with dynamical considerations (Biello et al. 2007; Khouider and Han 2013). The wavenumber-2–5 power is consistent with the addition of mesosynoptic

“muscle” to the MJO (Majda and Stechmann 2009) by slantwise overturning. Momentum transport and convective heating have similar effects on the Kelvin waves that are somewhat stronger but too weak compared to NCEP reanalysis.

The spontaneous generation of large-scale coherence in the aquaplanet simulations and the full GCM may

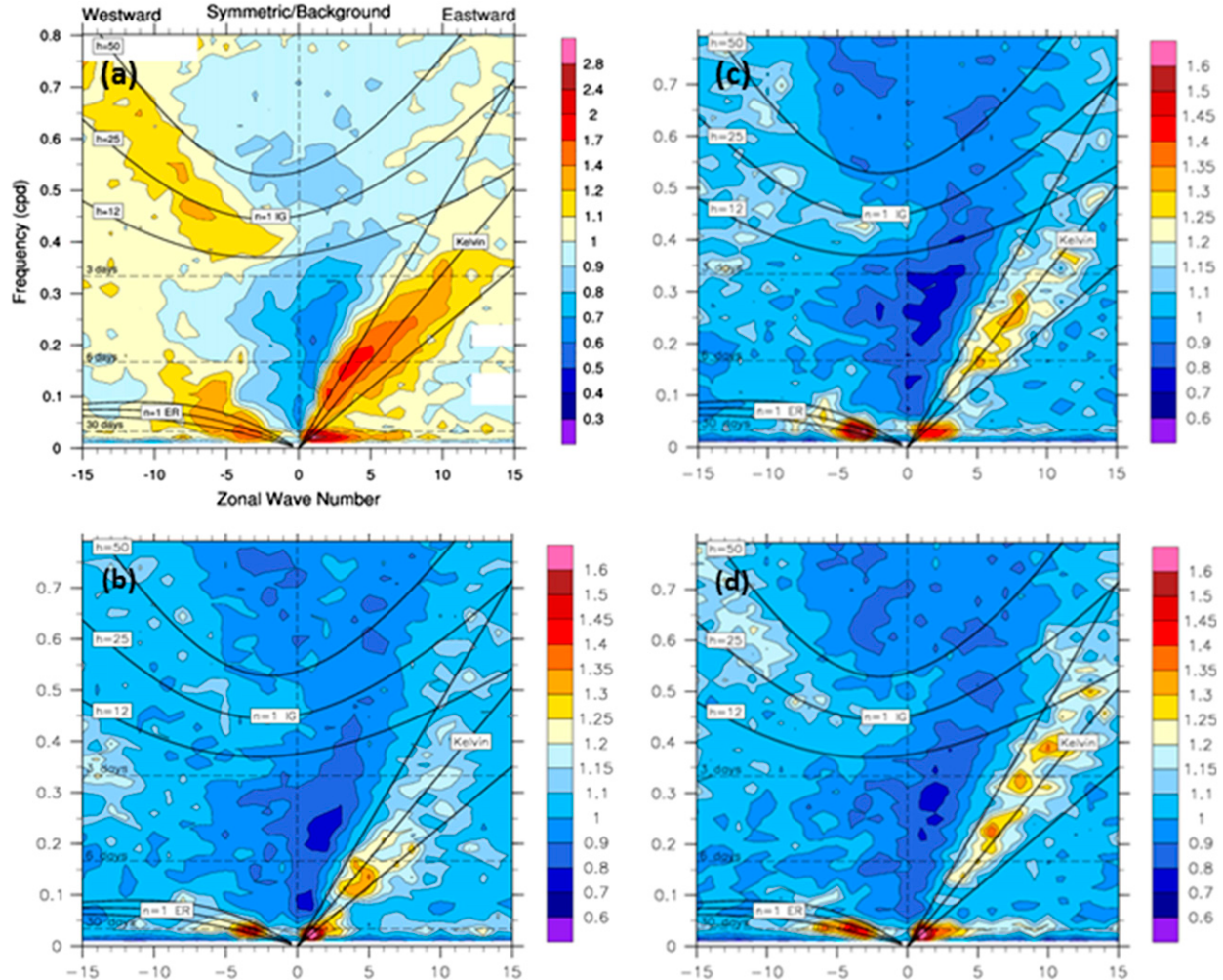


FIG. 15. Wheeler–Kiladis diagram for precipitation rate. (a) NCEP reanalysis. (b) CAM5.5 control. (c) MCSP momentum transport parameterization experiment, $\alpha_2 = 1.0 \text{ m s}^{-1} \text{ day}^{-1}$. (d) MCSP second-baroclinic heating experiment, $\alpha_1 = 1$.

involve new scale-selection principles. We refer to M04 (sections 8b and 8c) Moncrieff and Waliser (2015, sections 15.4.1 and 15.4.3) for more information.

6. Concluding remarks

Based on cloud-system simulation, dynamical analysis and a new paradigm for parameterizing convective organization in GCMs, we have quantified the following aspects:

- (i) Organized convective systems and their interaction with equatorial waves in a YOTC MJO event simulated by WRF.
- (ii) Nonlinear multiscale slantwise overturning models based on Lagrangian conservation principles for sheared environments approximate the simulated systems.
- (iii) Based on the separable relationship between vertical velocity and convective heating for cumulonimbus,

squall lines, superclusters, and convectively coupled equatorial waves, slantwise overturning displays self-similar properties.

- (iv) Utilized as MCSP transport modules, the slantwise overturning models generate large-scale patterns of tropical precipitation, notably in the Indian Ocean–western Pacific warm pool and the adjoining regions.
- (v) MCSP is the first unambiguous measure of the large-scale effects of organized tropical convection, a principal objective of the parameterization of organized convection described herein.
- (vi) The slantwise overturning models are expressed in system-relative (Lagrangian) coordinates whereas traditional convection parameterizations are in Eulerian coordinates; therefore, MCSP represents the observed propagation of precipitating convective systems in sheared environments.

Much remains to be done with MCSP beyond the proof-of-concept studies addressed herein. The role of vertical shear in slantwise overturning is implicit in the rearward slant of the airflow and the second-baroclinic mesoscale heating and convective momentum transport. The sign of convective momentum transport depends on the direction of propagation of the convective system and the shear vector. Negative momentum transport for eastward-moving systems (e.g., Fig. 12) was applied universally herein. However, important categories of organized convection are associated with positive momentum transport. An excellent example is the westward-moving West African squall lines and MCSs in association with easterly waves. Priorities for MCSP are to add shear direction to the convective momentum transport tendency and selective application of the α_2 parameter. This should enable meaningful observational evaluation of simulated large-scale convective coherence for different tropical wave categories.

Longer-term research and GCM experiments include the following: (i) observational analysis to provide realistic values for the α parameters, (ii) utilize the Majda (2007) mesoscale equatorial synoptic dynamical (MESD) model to parameterize upscale effects of organized tropical convection and quantify the role of slantwise overturning in convectively coupled waves, (iii) utilize the Khouider–Majda multicloud model (MCM) to address how slantwise overturning generates large-scale convective coherence, (iv) utilize MCM and MCSD to investigate new scale-selection mechanisms, and (v) implement MCSP in other GCMs, noting that MCSP's computational efficiency will enable utilization in coupled models, ensemble prediction systems, and Earth system models.

Finally, while real global field campaigns are fiscally and logistically out of the question, mesoscale data are required to evaluate the physical and dynamical effects of convective organization. The YOTC project pioneered the virtual global field-campaign concept in the form of ECMWF IFS global analyses, forecasts, and subgrid tendencies at 25-km grid spacing. As a contribution to the Year of Polar Prediction (YOPP; <http://www.polarprediction.net/yopp.html>), the ECMWF has, since November 2016, provided output data at 18-km grid spacing from the control simulation of their ensemble prediction system coupled to a $1/4^\circ$ ocean and a sea-ice model. It is anticipated that 9-km global data will be available to YOPP once coupling is added to the IFS in a year or so (P. Bauer, ECMWF, 2017, personal communication). These unique “observations” will also be useful for Years of the Maritime Continent (YMC) purposes where organized convection, ocean coupling, and complex orography are important research issues.

Acknowledgments. Mitch Moncrieff and Changhai Liu acknowledge NASA Grant NNX13AO39G: Diagnostic Analysis and Cloud-System Modeling of Organized Tropical Convection in the YOTC-ECMWF Database to Develop Climate Model Parameterizations, specifically subcontract 49A03A from the City College of New York, and Professor William Rossow as the principal investigator. Thanks to two anonymous reviewers for helpful comments that significantly improved the presentation of this paper.

REFERENCES

- Arakawa, A., and W. H. Schubert, 1974: Interaction of a cumulus cloud ensemble with the large-scale environment, part I. *J. Atmos. Sci.*, **31**, 674–701, doi:[10.1175/1520-0469\(1974\)031<0674:IOACCE>2.0.CO;2](https://doi.org/10.1175/1520-0469(1974)031<0674:IOACCE>2.0.CO;2).
- Berner, J., G. Shutts, M. Leutbecher, and T. Palmer, 2009: A spectral stochastic kinetic energy backscatter scheme and its impact on flow-dependent predictability in the ECMWF ensemble prediction system. *J. Atmos. Sci.*, **66**, 603–626, doi:[10.1175/2008JAS2677.1](https://doi.org/10.1175/2008JAS2677.1).
- Biello, J., A. Majda, and M. W. Moncrieff, 2007: Meridional momentum flux and superrotation in the multiscale IPESD MJO model. *J. Atmos. Sci.*, **64**, 1636–1651, doi:[10.1175/JAS3908.1](https://doi.org/10.1175/JAS3908.1).
- , B. Khouider, and A. J. Majda, 2010: Stochastic models for convective momentum transport. *Commun. Math. Sci.*, **8**, 187–216, doi:[10.4310/CMS.2010.v8.n1.a10](https://doi.org/10.4310/CMS.2010.v8.n1.a10).
- Bogenschutz, P. A., A. Gettelman, H. Morrison, V. E. Larson, C. Craig, and D. P. Schannen, 2013: Higher-order turbulence closure and its impact on climate simulations in the Community Atmosphere Model. *J. Climate*, **26**, 9655–9676, doi:[10.1175/JCLI-D-13-00075.1](https://doi.org/10.1175/JCLI-D-13-00075.1).
- Chen, F., and J. Dudhia, 2001: Coupling an advanced land surface–hydrology model with the Penn State–NCAR MM5 modeling system. Part I: Model description and implementation. *Mon. Wea. Rev.*, **129**, 569–585, doi:[10.1175/1520-0493\(2001\)129<0569:CAALSH>2.0.CO;2](https://doi.org/10.1175/1520-0493(2001)129<0569:CAALSH>2.0.CO;2).
- Donner, L. J., 1993: A cumulus parameterization including mass fluxes, vertical momentum dynamics, and mesoscale effects. *J. Atmos. Sci.*, **50**, 889–906, doi:[10.1175/1520-0469\(1993\)050<0889:ACPIMF>2.0.CO;2](https://doi.org/10.1175/1520-0469(1993)050<0889:ACPIMF>2.0.CO;2).
- , C. J. Seman, R. S. Hemler, and S. M. Fan, 2001: A cumulus parameterization including mass fluxes, convective vertical velocities, and mesoscale effects: Thermodynamic and hydrological aspects in a general circulation model. *J. Climate*, **14**, 3444–3463, doi:[10.1175/1520-0442\(2001\)014<3444:ACPIMF>2.0.CO;2](https://doi.org/10.1175/1520-0442(2001)014<3444:ACPIMF>2.0.CO;2).
- Gerard, L., 2015: Model resolution issues and new approaches in the convection-permitting regions. *Seamless Prediction of the Earth-System: From Minutes to Months*, G. Brunet, S. Jones, and P. M. Rutledge, Eds., World Meteorological Organization, 113–134. [Available online at http://library.wmo.int/pmb_ged/wmo_1156_en.pdf.]
- Golaz, J.-C., V. E. Larson, and W. R. Cotton, 2002: A PDF-based model for boundary layer clouds. Part I: Method and model description. *J. Atmos. Sci.*, **59**, 3540–3551, doi:[10.1175/1520-0469\(2002\)059<3540:APBMFB>2.0.CO;2](https://doi.org/10.1175/1520-0469(2002)059<3540:APBMFB>2.0.CO;2).
- Grabowski, W. W., 2001: Coupling cloud processes with the large-scale dynamics using the Cloud-Resolving Convection

- Parameterization (CRCP). *J. Atmos. Sci.*, **58**, 978–997, doi:[10.1175/1520-0469\(2001\)058<0978:CCPWTL>2.0.CO;2](https://doi.org/10.1175/1520-0469(2001)058<0978:CCPWTL>2.0.CO;2).
- Haertel, P. T., and R. H. Johnson, 1998: Two-day disturbances in the equatorial western Pacific. *Quart. J. Roy. Meteor. Soc.*, **124**, 615–636, doi:[10.1002/qj.49712454611](https://doi.org/10.1002/qj.49712454611).
- , and G. N. Kiladis, 2004: Dynamics of 2-day equatorial waves. *J. Atmos. Sci.*, **61**, 2707–2721, doi:[10.1175/JAS3352.1](https://doi.org/10.1175/JAS3352.1).
- Hartmann, D. L., H. H. Hendon, and R. A. Houze Jr., 1984: Some implications of the mesoscale circulations in tropical cloud clusters for large-scale dynamics and climate. *J. Atmos. Sci.*, **41**, 113–121, doi:[10.1175/1520-0469\(1984\)041<0113:SIOTMC>2.0.CO;2](https://doi.org/10.1175/1520-0469(1984)041<0113:SIOTMC>2.0.CO;2).
- Haertel, P. T., G. N. Kilasis, A. Enno, and T. M. Rickenbach, 2008: Vertical-mode decomposition of 2-day waves and the Madden-Julian oscillation. *J. Atmos. Sci.*, **65**, 813–933, doi:[10.1175/2007JAS2314.1](https://doi.org/10.1175/2007JAS2314.1).
- Hong, S.-Y., Y. Noh, and J. Dudhia, 2006: A new vertical diffusion package with an explicit treatment of entrainment processes. *Mon. Wea. Rev.*, **134**, 2318–2341, doi:[10.1175/MWR3199.1](https://doi.org/10.1175/MWR3199.1).
- Houze, R. A., Jr., 2004: Mesoscale convective systems. *Rev. Geophys.*, **42**, RG4003, doi:[10.1029/2004RG000150](https://doi.org/10.1029/2004RG000150).
- , 2014: *Cloud Dynamics*. 2nd ed. International Geophysics Series, Vol. 14, Academic Press, 432 pp.
- , and A. K. Betts, 1981: Convection in GATE. *Rev. Geophys. Space Phys.*, **19**, 541–576, doi:[10.1029/RG019i004p00541](https://doi.org/10.1029/RG019i004p00541).
- , C.-P. Cheng, C. A. Leary, and J. Gamache, 1980: Diagnosis of cloud mass and heat flux from radar and synoptic data. *J. Atmos. Sci.*, **37**, 754–773, doi:[10.1175/1520-0469\(1980\)037<0754:DOCMAH>2.0.CO;2](https://doi.org/10.1175/1520-0469(1980)037<0754:DOCMAH>2.0.CO;2).
- Iacono, M. J., J. S. Delamere, E. J. Mlawer, M. W. Shephard, S. A. Clough, and W. D. Collins, 2008: Radiative forcing by long-lived greenhouse gases: Calculations with the AER radiative transfer models. *J. Geophys. Res.*, **113**, D13103, doi:[10.1029/2008JD009944](https://doi.org/10.1029/2008JD009944).
- Johnson, R. H., T. M. Rickenbach, S. A. Rutledge, P. E. Ciesielski, and W. H. Schubert, 1999: Trimodal characteristics of tropical convection. *J. Climate*, **12**, 2397–2418, doi:[10.1175/1520-0442\(1999\)012<2397:TCOTC>2.0.CO;2](https://doi.org/10.1175/1520-0442(1999)012<2397:TCOTC>2.0.CO;2).
- Kershaw, R., and D. Gregory, 1997: Parameterization of momentum transport by convection. Part I: Theory and cloud modelling results. *Quart. J. Roy. Meteor. Soc.*, **123**, 1133–1151, doi:[10.1002/qj.49712354102](https://doi.org/10.1002/qj.49712354102).
- Khairoutdinov, M., D. Randall, and C. Mott, 2005: Simulations of the atmospheric general circulation using a cloud-resolving model as a superparameterization of physical processes. *J. Atmos. Sci.*, **62**, 2136–2154, doi:[10.1175/JAS3453.1](https://doi.org/10.1175/JAS3453.1).
- Khouider, B., and A. J. Majda, 2006: A simple multicloud parameterization for convectively coupled tropical waves. Part I: Linear analysis. *J. Atmos. Sci.*, **63**, 1308–1323, doi:[10.1175/JAS3677.1](https://doi.org/10.1175/JAS3677.1).
- , and —, 2007: A simple multicloud parameterization for convectively coupled tropical waves. Part II: Nonlinear simulations. *J. Atmos. Sci.*, **64**, 381–400, doi:[10.1175/JAS3833.1](https://doi.org/10.1175/JAS3833.1).
- , and —, 2008: Multicloud models for organized tropical convection: Enhanced congestus heating. *J. Atmos. Sci.*, **65**, 895–914, doi:[10.1175/2007JAS2408.1](https://doi.org/10.1175/2007JAS2408.1).
- , and Y. Han, 2013: A framework for assessing the effects of mesoscales on synoptic scales. *Theor. Comput. Fluid Dyn.*, **27**, 473–489, doi:[10.1007/s00162-012-0276-8](https://doi.org/10.1007/s00162-012-0276-8).
- , and M. W. Moncrieff, 2015: Organized convection parameterization for the ITCZ. *J. Atmos. Sci.*, **72**, 3073–3096, doi:[10.1175/JAS-D-15-0006.1](https://doi.org/10.1175/JAS-D-15-0006.1).
- Kiladis, G. N., M. C. Wheeler, P. T. Haertel, K. H. Straub, and P. E. Roundy, 2009: Convectively coupled equatorial waves. *Rev. Geophys.*, **47**, RG2003, doi:[10.1029/2008RG000266](https://doi.org/10.1029/2008RG000266).
- Lafore, J.-P., and M. W. Moncrieff, 1989: A numerical investigation of the organization and interaction of the convective and stratiform regions of tropical squall lines. *J. Atmos. Sci.*, **46**, 521–544, doi:[10.1175/1520-0469\(1989\)046<0521:ANIOTO>2.0.CO;2](https://doi.org/10.1175/1520-0469(1989)046<0521:ANIOTO>2.0.CO;2).
- Lane, T. P., and M. W. Moncrieff, 2015: Long-lived convective systems in a low-convective inhibition environment. Part I: Upshear propagation. *J. Atmos. Sci.*, **72**, 4297–4318, doi:[10.1175/JAS-D-15-0073.1](https://doi.org/10.1175/JAS-D-15-0073.1).
- Lin, J., B. Mapes, M. Zhang, and M. Newman, 2004: Stratiform precipitation, vertical heating profiles, and the Madden-Julian oscillation. *J. Atmos. Sci.*, **61**, 296–309, doi:[10.1175/1520-0469\(2004\)061<0296:SPVHPA>2.0.CO;2](https://doi.org/10.1175/1520-0469(2004)061<0296:SPVHPA>2.0.CO;2).
- Majda, A. J., 2007: New multiscale models and self-similarity in tropical convection. *J. Atmos. Sci.*, **64**, 1393–1404, doi:[10.1175/JAS3880.1](https://doi.org/10.1175/JAS3880.1).
- , and S. N. Stechmann, 2009: The skeleton of tropical intra-seasonal oscillations. *Proc. Natl. Acad. Sci. USA*, **106**, 8417–8422, doi:[10.1073/pnas.0903367106](https://doi.org/10.1073/pnas.0903367106).
- Mapes, B. E., and R. Neale, 2011: Parameterizing convective organization to escape the entrainment dilemma. *J. Adv. Model. Earth Syst.*, **3**, M06004, doi:[10.1029/2011MS000042](https://doi.org/10.1029/2011MS000042).
- , S. N. Tulich, J.-L. Lin, and P. Zuidema, 2006: The mesoscale convection life cycle: Building block or prototype for large-scale tropical waves. *Dyn. Atmos. Oceans*, **42**, 3–29, doi:[10.1016/j.dynatmoc.2006.03.003](https://doi.org/10.1016/j.dynatmoc.2006.03.003).
- Matsuno, T., 1966: Quasi-geostrophic motions in the equatorial area. *J. Meteor. Soc. Japan*, **44**, 25–43.
- Miyakawa, T., Y. N. Takayabu, T. Nasuno, H. Miura, M. Satoh, and M. W. Moncrieff, 2012: Convective momentum transport by rainbands within a Madden-Julian oscillation in a global nonhydrostatic model with explicit deep convective processes. Part I: Methodology and general results. *J. Atmos. Sci.*, **69**, 1317–1338, doi:[10.1175/JAS-D-11-024.1](https://doi.org/10.1175/JAS-D-11-024.1).
- Moncrieff, M. W., 1981: A theory of organized steady convection and its transport properties. *Quart. J. Roy. Meteor. Soc.*, **107**, 29–50, doi:[10.1002/qj.49710745103](https://doi.org/10.1002/qj.49710745103).
- , 1992: Organized convective systems: Archetypal models, mass and momentum flux theory, and parameterization. *Quart. J. Roy. Meteor. Soc.*, **118**, 819–850, doi:[10.1002/qj.49711850703](https://doi.org/10.1002/qj.49711850703).
- , 1997: Momentum transport by organized convection. *The Physics and Dynamics on Moist Atmospheric Convection*, R. K. Smith, Ed., NATO ASI Series, Series C: Mathematical and Physical Sciences, Vol. 505, Kluwer Academic Publishers, 231–253.
- , 2004: Analytic representation of the large-scale organization of tropical convection. *J. Atmos. Sci.*, **61**, 1521–1538, doi:[10.1175/1520-0469\(2004\)061<1521:AROTLO>2.0.CO;2](https://doi.org/10.1175/1520-0469(2004)061<1521:AROTLO>2.0.CO;2).
- , 2010: The multiscale organization of moist convection and the intersection of weather and climate. *Climate Dynamics: Why Does Climate Vary? Geophys. Monogr.*, Vol. 189, Amer. Geophys. Union, 3–26, doi:[10.1029/2008GM000838](https://doi.org/10.1029/2008GM000838).
- , and J. S. A. Green, 1972: The propagation and transfer properties of steady convective overturning in shear. *Quart. J. Roy. Meteor. Soc.*, **98**, 336–352, doi:[10.1002/qj.49709841607](https://doi.org/10.1002/qj.49709841607).
- , and E. Klinker, 1997: Organized convective systems in the tropical western Pacific as a process in general circulation models. *Quart. J. Roy. Meteor. Soc.*, **123**, 805–828, doi:[10.1002/qj.49712354002](https://doi.org/10.1002/qj.49712354002).
- , and C. Liu, 2006: Representing convective organization in prediction models by a hybrid strategy. *J. Atmos. Sci.*, **63**, 3404–3420, doi:[10.1175/JAS3812.1](https://doi.org/10.1175/JAS3812.1).
- , and D. E. Waliser, 2015: Organized convection and the YOTC Project. *Seamless Prediction of the Earth-System: From*

- Minutes to Months*, G. Brunet, S. Jones, and P. M. Ruti, Eds., World Meteorological Organization, 283–310. [Available online at http://library.wmo.int/pmb_ged/wmo_1156_en.pdf.]
- , —, M. J. Miller, M. E. Shapiro, G. Asrar, and J. Caughey, 2012: Multiscale convective organization and the YOTC Virtual Global Field Campaign. *Bull. Amer. Meteor. Soc.*, **93**, 1171–1187, doi:[10.1175/BAMS-D-11-00233.1](https://doi.org/10.1175/BAMS-D-11-00233.1).
- Nakazawa, T., 1988: Tropical superclusters within intraseasonal variations over the western Pacific. *J. Meteor. Soc. Japan*, **66**, 823–839.
- Neale, R. B., and Coauthors, 2012: Description of the NCAR Community Atmosphere Model (CAM 5.0). NCAR Tech. Note NCAR/TN-486+STR, 274 pp. [Available online at http://www.cesm.ucar.edu/models/cesm1.0/cam/docs/description/cam5_desc.pdf.]
- Nesbitt, S. W., R. Cifelli, and S. A. Rutledge, 2006: Storm morphology and rainfall characteristics of TRMM precipitation features. *Mon. Wea. Rev.*, **134**, 2702–2721, doi:[10.1175/MWR3200.1](https://doi.org/10.1175/MWR3200.1).
- Oh, J.-H., X. Jiang, D. E. Waliser, M. W. Moncrieff, R. H. Johnson, and P. Ciesielski, 2015: A momentum budget analysis of westerly winds events associated with the Madden-Julian oscillation during DYNAMO. *J. Atmos. Sci.*, **72**, 3780–3799, doi:[10.1175/JAS-D-15-0044.1](https://doi.org/10.1175/JAS-D-15-0044.1).
- Richter, J. H., and P. J. Rasch, 2008: Effects of convective momentum transport on the atmospheric circulation in the Community Atmosphere Model, version 3. *J. Climate*, **21**, 1487–1499, doi:[10.1175/2007JCLI1789.1](https://doi.org/10.1175/2007JCLI1789.1).
- Schumacher, C., R. A. Houze Jr., and I. Kraucunas, 2004: The tropical dynamical response to latent heating estimates derived from the TRMM precipitation radar. *J. Atmos. Sci.*, **61**, 1341–1358, doi:[10.1175/1520-0469\(2004\)061<1341:TTDRTL>2.0.CO;2](https://doi.org/10.1175/1520-0469(2004)061<1341:TTDRTL>2.0.CO;2).
- Straub, K. H., and G. N. Kiladis, 2002: Observations of a convectively coupled Kelvin wave in the eastern Pacific ITCZ. *J. Atmos. Sci.*, **59**, 30–53, doi:[10.1175/1520-0469\(2002\)059<0030:OOACCK>2.0.CO;2](https://doi.org/10.1175/1520-0469(2002)059<0030:OOACCK>2.0.CO;2).
- Takayabu, Y. N., 1994: Large-scale cloud disturbances associated with equatorial waves. Part II: Westward-propagating inertio-gravity waves. *J. Meteor. Soc. Japan*, **72**, 451–465.
- , K.-M. Lau, and C. H. Sui, 1996: Observation of a quasi-2-day wave during TOGA COARE. *Mon. Wea. Rev.*, **124**, 1892–1912, doi:[10.1175/1520-0493\(1996\)124<1892:OOAQDW>2.0.CO;2](https://doi.org/10.1175/1520-0493(1996)124<1892:OOAQDW>2.0.CO;2).
- Tao, W.-K., and M. W. Moncrieff, 2009: Multiscale cloud system modeling. *Rev. Geophys.*, **47**, RG4002, doi:[10.1029/2008RG000276](https://doi.org/10.1029/2008RG000276).
- Thompson, G., P. R. Field, W. R. Hall, and R. M. Rasmussen, 2008: Explicit forecasts of winter precipitation using an improved bulk microphysics scheme. Part II: Implementation of a new snow parameterization. *Mon. Wea. Rev.*, **136**, 5095–5115, doi:[10.1175/2008MWR2387.1](https://doi.org/10.1175/2008MWR2387.1).
- Tung, W.-W., and M. Yanai, 2002: Convective momentum transport observed during the TOGA COARE IOP. Part II: Case studies. *J. Atmos. Sci.*, **59**, 2535–2549, doi:[10.1175/1520-0469\(2002\)059<2535:CMTODT>2.0.CO;2](https://doi.org/10.1175/1520-0469(2002)059<2535:CMTODT>2.0.CO;2).
- Vitart, F., 2014: Evolution of the ECMWF sub-forecast skill scores. *Quart. J. Roy. Meteor. Soc.*, **140**, 1889–1899, doi:[10.1002/qj.2256](https://doi.org/10.1002/qj.2256).
- , and Coauthors, 2015: Sub-seasonal to seasonal prediction: Linking weather and climate. *Seamless Prediction of the Earth-System: From Minutes to Months*, G. Brunet, S. Jones, and P. M. Ruti, Eds., World Meteorological Organization, 385–401. [Available online at http://library.wmo.int/pmb_ged/wmo_1156_en.pdf.]
- Waliser, D. E., and Coauthors, 2012: The “Year” of Tropical Convection (May 2008–April 2010): Climate variability and weather highlights. *Bull. Amer. Meteor. Soc.*, **93**, 1189–1218, doi:[10.1175/2011BAMS3095.1](https://doi.org/10.1175/2011BAMS3095.1).
- Wheeler, M., and G. N. Kiladis, 1999: Convectively coupled equatorial waves: Analysis of clouds and temperature in the wavenumber-frequency domain. *J. Atmos. Sci.*, **56**, 374–399, doi:[10.1175/1520-0469\(1999\)056<0374:CCEWAO>2.0.CO;2](https://doi.org/10.1175/1520-0469(1999)056<0374:CCEWAO>2.0.CO;2).
- Wu, X., and M. Yanai, 1994: Effects of wind shear on the cumulus transport of momentum: Observations and parameterization. *J. Atmos. Sci.*, **51**, 1640–1660, doi:[10.1175/1520-0469\(1994\)051<1640:EOVWSO>2.0.CO;2](https://doi.org/10.1175/1520-0469(1994)051<1640:EOVWSO>2.0.CO;2).
- Xie, S., H. Ma, J. Boyle, S. Klein, and Y. Zhang, 2012: On the correspondence between short- and long-time-scale systematic errors in CAM4/CAM5 for the Years of Tropical Convection. *J. Climate*, **25**, 7937–7955, doi:[10.1175/JCLI-D-12-00134.1](https://doi.org/10.1175/JCLI-D-12-00134.1).
- Yano, J.-I., and M. W. Moncrieff, 2016: Numerical archetypal parameterization for mesoscale convective systems. *J. Atmos. Sci.*, **73**, 2585–2602, doi:[10.1175/JAS-D-15-0207.1](https://doi.org/10.1175/JAS-D-15-0207.1).
- , J. C. McWilliams, M. W. Moncrieff, and K. A. Emanuel, 1995: Hierarchical tropical cloud systems in an analog shallow-water model. *J. Atmos. Sci.*, **52**, 1723–1742, doi:[10.1175/1520-0469\(1995\)052<1723:HTCSIA>2.0.CO;2](https://doi.org/10.1175/1520-0469(1995)052<1723:HTCSIA>2.0.CO;2).
- Zhang, G. J., and N. A. McFarlane, 1995: Sensitivity of climate simulations to the parameterization of cumulus convection in the Canadian Climate General Circulation Model. *Atmos.–Ocean*, **33**, 407–446, doi:[10.1080/07055900.1995.9649539](https://doi.org/10.1080/07055900.1995.9649539).